Crystal structure and magnetic properties of lanthanide-*trans*-2-butenoate polymers (Ln = La, Pr, Dy, Ho)

Ricardo Baggio [a], Maria T. Garland [b], Octavio Peña [c], Mireille Perec [d,*]

[a] *Departamento de Física, Comisión Nacional de Energía Atómica, Av. Gral Paz 1499, 1650 San Martín, Buenos Aires, Argentina*
[b] *Departamento de Física, Facultad de Ciencias Físicas y Matemáticas, Universidad de Chile, CIMAT, Avda. Blanco Encalada 2008, Casilla 487-3, Santiago, Chile*
[c] *U.M.R. 6511, L.C.S.I.M. CNRS. Institut de Chimie de Rennes, Université de Rennes 1, 35042 Rennes, France*
[d] *Departamento de Química Inorgánica Analítica y Química Física, Facultad de Ciencias Exactas y Naturales, INQUIMAE, Universidad de Buenos Aires, Ciudad Universitaria, Pabellón II, C1428EHA, 1428 Buenos Aires, Argentina*

Abstract

Four lanthanide coordination polymers formulated as $\{[La_3L_9(H_2O)_3]EtOH\cdot H_2O\}_n$ **1**, $\{[Pr_2L_6(H_2O)_2]HL\cdot H_2O\}_n$ **2**, $\{[Dy_2L_6(H_2O)]0.5HL\cdot H_2O\}_n$ **3** and $\{[Ho_2L_6(H_2O)]0.5HL\cdot H_2O\}_n$ **4** and HL = *trans*-2-butenoic acid have been synthesized from the corresponding pure lanthanide oxide and HL acid in water at pH 3. The compounds were characterized by chemical analysis, IR spectroscopy, thermogravimetry, variable-temperature magnetic susceptibility and single crystal X-ray diffraction studies. A common feature in these materials is the presence of two differentiated lanthanide nodes linked by carboxylates into extended chains. These are further connected by inter- and intra-molecular hydrogen-bonds involving ligand and solvate molecules. Weak ferromagnetic interactions appear to be operative in the Dy material.

Keywords: Crystal structures; Lanthanide(III) carboxylates; Magnetic properties

1. Introduction

The construction of extended frameworks containing f-elements bridged by carboxylate groups has attracted a great deal of interest because of the large variety of architectures that result from the high and variable coordination numbers of the metal centers as well as of the coordination versatility of the carboxylate ligands [1–6]. Unique properties may also result from their photophysical behavior [7–9] as well as from their generally large anisotropic magnetic moments [10,11]. Recent studies on the olefinic monocarboxylate *trans*-2-butenoate (hereafter called L) as a building block for Eu, Gd, Tb and Nd showed that the ligand is able to stabilize different coordination polymers and oligomers. The europium polymer $[Eu_3L_9(H_2O)_4\cdot(H_2O)\cdot(EtOH)]_n$ [12] shows three independent metal centers linked to each other by three different types and number of carboxylate bridges, the gadolinium compound $[Gd_2L_6(H_2O)_4\cdot 2(H_2O)]$ [13] consists of two independent dimers in the unit cell, one doubly and the other quadruply bridged, the terbium polymer $[TbL_3(H_2O)\cdot(HL)]_n$ [12] shows one independent metal center bridged by double carboxylates and the neodymium polymer $[Nd_2L_6(H_2O)_3]_n$ [14] is built up around two independent metal centers, one 9- and one 10-coordinate, bridged in two different modes by two pairs of oxygen atoms from chelating-bridging carboxylates.

* Corresponding author. Tel.: +54 11 4576 3358; fax: +54 11 4576 3341.
E-mail address: perec@q1.fcen.uba.ar (M. Perec).

The structural variety obtained for the Ln-*trans*-2-butenoate compounds prompted us to further study this series. Herein, we report the preparation, structural characterization and magnetic behavior in the temperature range 2–300 K of four novel binary complexes formulated as $[La_3L_9(H_2O)_3\cdot(EtOH)\cdot(H_2O)]_n$ **1**, $[Pr_2L_6(H_2O)_2\cdot(HL)\cdot(H_2O)]_n$ **2** and $[Ln_2L_6(H_2O)\cdot 0.5(HL)\cdot(H_2O)]_n$, where Ln = Dy **3** and Ho **4**.

2. Experimental

2.1. Materials and methods

All starting materials were purchased from Aldrich and used without further purification. Elemental analyses (C, H) were performed on a Carlo Erba EA 1108 instrument. Infrared spectra were recorded on a Nicolet FT-IR 510 P spectrophotometer using the KBr pellet technique. Thermogravimetric analyses were recorded on a Shimadzu DTG-50 thermal analyzer, under an atmosphere of air at a heating rate of 5 °C min^{-1}. Powder X-ray diffraction (XRD) data were collected using monochromated Cu Kα radiation on a Phillips X'Pert diffractometer.

2.2. Preparations

2.2.1. $[\{La_3(MeCH{=}CHCO_2)_9(H_2O)_3\}\cdot MeCH{=}CHCO_2H\cdot H_2O]_n$ (1)

La_2O_3 (0.33 g, 1 mmol) was added to a solution of *trans*-2-butenoic acid (0.87 g, 10 mmol) in water (100 ml). The reaction mixture was heated under reflux for 4 h under continuous stirring and filtered while hot. The clear solution was stored at room temperature for three weeks whereupon a colorless crystalline powder was filtered off and dried in vacuum. Single crystals of **1** suitable for crystallographic work separated out from the filtered solution after standing for another four weeks. The yield was about 65% based on the amount of La_2O_3 used. *Anal.* Calc. for $C_{40}H_{59}O_{24}La_3$: C, 35.80; H, 4.40. Found: C, 35.95; H, 4.45%. Main FT IR bands (KBr, cm^{-1}): 3357vs,br, 3028w, 2968w, 2938w, 2913w, 2851w, 1660vs, 1515vs,br, 1453vs,br, 1294m, 1253m, 1103w, 1044vw, 970m, 915w, 856m, 743m, 697m, 528m, 415m.

2.2.2. $[\{Pr_2(MeCH{=}CHCO_2)_6(H_2O)\}\cdot MeCH{=}CHCO_2H\cdot H_2O]_n$ (2)

The same procedure using Pr_2O_3 instead of La_2O_3 (0.35 g, 1 mmol) afforded a crystalline powder and single crystals of **2**. Yield: 70%. *Anal.* Calc. for $C_{26}H_{42}O_{16}Pr_2$: C, 34.95; H, 4.70. Found: C, 35.0; H, 4.60%. The FT IR spectrum was similar within ±10 cm^{-1} to that mentioned above.

2.2.3. $[\{Dy_2(MeCH{=}CHCO_2)_6(H_2O)\}\cdot 0.5\ MeCH{=}CHCO_2H.H_2O]_n$ (3)

$Dy_2(CO_3)_3\cdot xH_2O$ (0.51 g, 1 mmol) was added to a solution of *trans*-2-butenoic acid (0.52 g, 6 mmol) in water (70 ml). The reaction mixture was stirred under reflux for 1 h under continuous stirring and filtered while hot. The clear solution at pH 2.5–3.0 was stored for three weeks, whereupon colorless crystals of the product suitable for X-ray analysis were collected by filtration and dried in air, Yield 65%. *Anal.* Calc. for $C_{26}H_{43}Dy_2O_{18}$: C, 32.20; H, 4.47. Found: C, 32.25; H, 4.40%. The FT IR spectrum was similar within ±10 cm^{-1} to those mentioned above.

2.2.4. $[\{Ho_2(MeCH{=}CHCO_2)_6(H_2O)\}\cdot 0.5\ MeCH{=}CHCO_2H.H_2O]_n$ (4)

The same procedure using $Ho_2(CO_3)_3\cdot xH_2O$ instead of $Dy_2(CO_3)_3\cdot xH_2O$ afforded a crystalline powder and single crystals of **4**. Yield: 70%. *Anal.* Calc. for $C_{26}H_{43}Ho_2O_{18}$: C, 32.05; H, 4.45. Found 32.00; H, 4.40%. The FT IR spectrum was similar within ±10 cm^{-1} to those mentioned above. The X-ray powder diffraction data showed this compound to be isostructural to **3**.

2.3. X-ray crystallography

Single crystal X-ray diffraction data were collected on a Siemens R3m four circle diffractometer, using graphite monochromatized Mo Kα radiation, $\lambda = 0.71069$ Å, scan type $\omega/2$, corrected for absorption via ψ scan (structures **1**, **2** and **3**). Structure **4** was measured on a Bruker AXS SMART APEX CCD diffractometer also using graphite monochromatized Mo Kα radiation, with SMART [15] as the driving software and data integration performed using SAINT [16]. A semiempirical absorption correction was applied.

The structures were solved by direct methods and difference Fourier, and refined by least squares on F^2 with anisotropic displacement parameters for non-H atoms. Hydrogen atoms defined by the stereochemistry were placed at their calculated positions and allowed to ride onto their host carbons both in coordinates as well as in thermal parameters. Those attached to oxygen were found in the final difference Fourier maps and refined with a restrained O–H distance (0.94 Å), except in the case of the pair O(2E)–H(2E) (see discussion below). All calculations to solve the structures, refine the models proposed and obtain derived results were carried out with the computer programs SHELXS-97 and SHELXL-97 [17] and SHELXTL [18]. Full use of the CCDC package was also made for searching in the CSD Database [19].

A summary of crystal parameters and data collection and refinement details is given in Table 1. Tables 2, 4, and 6 provide selected bond parameters, while Tables 3, 5 and 7 present those for H-bonding interactions.

Table 1
Crystallographic and refinement data for **1**, **2**, **3** and **4**

Code	(**1**)	(**2**)	(**3**)	(**4**)
Empirical formula	$C_{40}H_{59}La_3O_{24}$	$C_{26}H_{42}O_{16}Pr_2$	$C_{26}H_{43}Dy_2O_{18}$	$C_{26}H_{43}Ho_2O_{18}$
Formula weight	1340.6	892.41	968.60	973.46
Crystal system/space group	monoclinic; $P2_1/c$	monoclinic; $P2_1/c$	monoclinic; $P2_1/c$	monoclinic; $P2_1/c$
a (Å)	10.5318(15)	11.535(6)	7.926(3)	7.9009(9)
b (Å)	10.399(2)	14.401(7)	16.433(8)	16.4149(18)
c (Å)	24.810(4)	21.799(11)	28.366(14)	28.262(3)
β (°)	98.031(12)	97.94(4)	97.00(4)	97.465(2)
V (Å^3)	2690.5(8)	3586(3)	3667(3)	3634.3(7)
Z	2	4	4	4
d_{calc} (g cm^{-3})	1.654	1.653	1.754	1.779
μ (mm^{-1})	2.414	2.749	4.113	4.393
$F(000)$	1322	1776	1900	1908
Crystal size (mm^3)	$0.22 \times 0.18 \times 0.12$	$0.28 \times 0.16 \times 0.14$	$0.38 \times 0.08 \times 0.06$	$0.35 \times 0.03 \times 0.03$
θ range (°)	1.66–25.00.	1.70–25.02.	1.90–25.01	1.91–28.14.
Index range	$0 \leqslant h \leqslant 12$, $0 \leqslant k \leqslant 12$, $-29 \leqslant l \leqslant 29$	$-13 \leqslant h \leqslant 13$, $0 \leqslant k \leqslant 17$, $0 \leqslant l \leqslant 25$	$-9 \leqslant h \leqslant 9$, $0 \leqslant k \leqslant 19$, $0 \leqslant l \leqslant 33$	$-10 \leqslant h \leqslant 10$, $-21 \leqslant k \leqslant 21$, $-37 \leqslant l \leqslant 24$
Reflections collected	5023	6976	6987	21 009
Independent reflections [R_{int}]	4745 [0.040]	6310 [0.0497]	6389 [0.059]	8044 [0.076]
Data/parameters	4745/321	6310/426	6389/465	8044/465
Goodness-of-fit on F^2	1.009	0.975	0.920	0.910
Final R indices [$I > 2\sigma(I)$]	[a] $R_1 = 0.0487$, $wR_2 = 0.1369$	[a] $R_1 = 0.0511$, [b] $wR_2 = 0.0776$	[a] $R_1 = 0.0515$, [b] $wR_2 = 0.1160$	[a] $R_1 = 0.0524$, [b] $wR_2 = 0.0825$
R indices (all data)	[a] $R_1 = 0.0706$, [b] $wR_2 = 0.1537$	[a] $R_1 = 0.1018$, [b] $wR_2 = 0.0920$	[a] $R_1 = 0.1012$, [b] $wR_2 = 0.1458$	[a] $R_1 = 0.1451$, [b] $wR_2 = 0.1003$
Largest $\Delta\rho$ (e Å^{-3})	0.929 and −0.821	0.598 and −0.628	2.043 and −2.036	1.057 and −1.246

Common features: temperature, 293(2) K; wavelength: 0.71073 Å; crystal system; structure resolution: direct methods (SHELXS-97); structure refinement: full-matrix least-squares on F^2 (SHELXL-97).

[a] R_1: $\sum||F_o| - |F_c||/\sum|F_o|$.

[b] wR_2 : $[\sum[w(F_o^2 - F_c^2)^2]/\sum[w(F_o^2)^2]]^{1/2}$.

Table 2
Selected bond lengths and distances (Å) for **1**

La(1)–O(1B)	2.447(6)
La(1)–O(1B)#1	2.447(6)
La(1)–O(1C)	2.493(4)
La(1)–O(1C)#1	2.493(4)
La(1)–O(1D)#1	2.580(5)
La(1)–O(1D)	2.580(5)
La(1)–O(1W)	2.630(5)
La(1)–O(1W)#1	2.630(5)
La(1)–O(2D)	3.062(5)
La(2)–O(2D)	2.402(5)
La(2)–O(2A)#2	2.466(5)
La(2)–O(2B)	2.467(5)
La(2)–O(1E)	2.503(5)
La(2)–O(1A)	2.554(5)
La(2)–O(2C)	2.555(5)
La(2)–O(2W)	2.588(5)
La(2)–O(1C)	2.704(4)
La(2)–O(2A)	2.960(5)

Symmetry transformations used to generate equivalent atoms: #1 $-x + 1$, y, $-z + 1/2$; #2 $-x + 1$, $-y + 1$, $-z + 1$.

Table 3
Hydrogen bonds for **1** (Å and °)

D–H...A	d(H...A)	d(D...A)	∠(DHA)
O(1W)–H(1WA)...O(1A)	1.83	2.709(6)	155
O(1W)–H(1WB)...O(1D)#1	2.26	2.970(8)	132
O(2W)–H(2WA)...O(2C)#2	1.80	2.740(6)	176
O(2W)–H(2WB)...O(2E)#3	1.84	2.771(8)	171
O(2E)–H(2E)...O(2E)#3	1.226	2.451(9)	180

Symmetry transformations used to generate equivalent atoms: #1 $-x + 1$, y, $-z + 1/2$; #2 $-x + 1$, $-y + 1$, $-z + 1$; #3 $-x + 2$, $-y + 1$, $-z + 1$.

2.4. Magnetic susceptibility measurements

Temperature dependent magnetic susceptibilities of solid samples were recorded on a SHE-906 VTS SQUID susceptometer, between 2 and 300 K, under an applied field of 0.5 or 1 kOe (10^3 A m^{-1}), depending on the range of temperature. Due to the smaller signal expected for the lanthanum compound, a larger applied field (5 kOe) was used in that case. The magnetization data were corrected for the sample holder's contribution and the diamagnetic susceptibility of the core electrons using Pascal's constants.

3. Results and discussion

Polymers **1**–**4** were similarly obtained from the reactions of the corresponding Ln_2O_3 (99.99%) (Ln = La, Pr, Dy, Ho) with *trans*-2-butenoic acid (1:6) in water

Table 4
Selected bond lengths for **2** (Å)

Pr(1)–O(1A)	2.435(6)
Pr(1)–O(2E)#4	2.442(6)
Pr(1)–O(2W)	2.464(6)
Pr(1)–O(1W)	2.471(6)
Pr(1)–O(1F)	2.532(6)
Pr(1)–O(3W)	2.535(5)
Pr(1)–O(1B)	2.540(6)
Pr(1)–O(2B)	2.572(5)
Pr(1)–O(2F)	2.574(5)
Pr(2)–O(1E)	2.485(6)
Pr(2)–O(2F)#5	2.505(6)
Pr(2)–O(2A)	2.513(6)
Pr(2)–O(2B)	2.534(6)
Pr(2)–O(2D)	2.543(6)
Pr(2)–O(1C)	2.584(6)
Pr(2)–O(2C)	2.595(6)
Pr(2)–O(1A)	2.653(5)
Pr(2)–O(1D)	2.667(6)
Pr(2)–O(2E)	2.697(5)

Symmetry transformations used to generate equivalent atoms: #4 $-x+2$, $y-1/2$, $-z+1/2$; #5 $-x+2$, $y+1/2$, $-z+1/2$.

Table 5
Hydrogen bonds for **2** (Å and °)

D–H...A	*d*(H...A)	*d*(D...A)	∠(DHA)
O(1W)–H(1WA)...O(1X)	1.82	2.738(9)	164
O(1W)–H(1WB)...O(2C)#4	1.87	2.741(8)	154
O(2W)–H(2WA)...O(1C)	1.86	2.653(8)	141
O(2W)–H(2WB)...O(2D)#5	1.82	2.676(8)	150
O(3W)–H(3WA)...O(1D)	1.98	2.866(8)	157
O(3W)–H(3WB)...O(1X)	1.95	2.754(10)	143
O(1X)–H(1XO)...O(1D)#6	1.91	2.747(8)	179

Symmetry transformations used to generate equivalent atoms: #4 $-x+2$, $y-1/2$, $-z+1/2$; #5 $-x+2$, $y+1/2$, $-z+1/2$; #6 $-x+2$, $-y+2$, $-z$.

and subsequent work-up. The solids are stable in dry atmosphere at room temperature. Thermogravimetric analyses show that weight loss starts at 50 °C in all cases and thermal degradations occur in overlapping steps leading to the final residues in the range 550–600 °C, which correspond to complete combustions of the polymers to the respective Ln_2O_3 as shown in the X-ray powder diffraction patterns. Single crystal X-ray analysis has been carried out on complexes **1**–**4** and crystallographic data are given in Table 1. The *trans*-2-butenoates are found to bind to the lanthanide(III) cations in the different coordination modes illustrated in Scheme 1.

3.1. Crystal structures

Structure **1** consists of polymeric chains of lanthanum coordination polyhedra, running along [0 0 1]. The one-dimensional arrays are formed by two different types of lanthanum cations: La1, onto a twofold symmetry axis, and La2, in a general position. The former presents an

Table 6
Selected bond lengths and distances for **3** and **4** (Å)

	Ln = Dy	Ln = Ho
Ln(1)–O(1B)	2.307(8)	2.291(6)
Ln(1)–O(1C)	2.888(10)	2.976(7)
Ln(1)–O(2C)	2.415(8)	2.374(8)
Ln(1)–O(2D)#7	2.262(8)	2.235(6)
Ln(1)–O(2E)	2.320(9)	2.287(7)
Ln(1)–O(1F)	2.412(8)	2.377(7)
Ln(1)–O(2F)	2.757(8)	2.750(7)
Ln(1)–O(1W)	2.371(8)	2.330(7)
Ln(1)–O(2W)	2.433(9)	2.412(7)
Ln(2)–O(1A)	2.322(10)	2.289(8)
Ln(2)–O(1B)	2.678(8)	2.665(7)
Ln(2)–O(2B)	2.441(8)	2.424(7)
Ln(2)–O(1C)	2.269(8)	2.233(6)
Ln(2)–O(1D)	2.370(8)	2.340(7)
Ln(2)–O(2F)#8	2.282(8)	2.278(6)
Ln(2)–O(3W)	2.384(8)	2.355(7)
Ln(2)–O(4W)	2.379(8)	2.348(7)
Ln(2)–O(2D)	3.154(8)	3.234(7)
Ln(1)...Ln(2)	4.242(4)	4.233(3)
Ln(1)...Ln(2)#7	4.355(4)	4.363(3)

Symmetry transformations used to generate equivalent atoms: #7 $x+1$, y, z; #8 $x-1$, y, z.

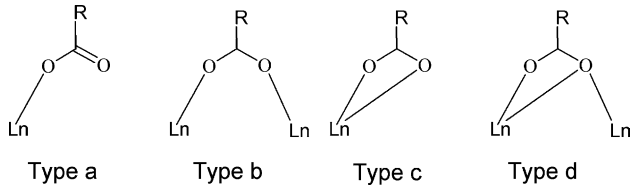

Scheme 1.

eightfold coordination built up through the binding of three bridging carboxylate groups (two type b, one type d), and one aqua O1W molecule providing one bond each, plus their symmetry related counterparts, Fig. 1.

The rather long La1...O2D distance of 3.062(5) Å, shown in broken lines in the figure, is not considered a coordination bond in the present description. La2 is 9-coordinated: four bonds are provided by two type d chelating ligands, other three by bridging carboxylates (two type b, one type d), a type a monodentate carboxylate and one aqua molecule O2W complete the coordination polyhedron.

There are two different La...La distances along the 1 D structure evolving along [1 0 0]. The first one, La1...La2, achieved via two carboxylato bridges (La1–O1B–C1B–O2B–La2 and La1–O1D–C1D–O2D–La2) and one oxygen bridge (La1–O1C–La2). The second, La2...La2#2, via one oxygen bridge (La2–O2A–La2#2) and its symmetry related one. The packing of the 1D arrays occurs through H-bonding interactions both intra and inter-chain, Fig. 2 and Table 3.

It should be noted that charge neutrality of the compound requires one half of the *trans*-2-butenoate to be

Table 7
Hydrogen bonds for **3** and **4** (Å and °)

D–H...A	*d*(H...A)		*d*(D...A)		∠(DHA)	
O(1W)–H(1WA)...O(2B)#7	1.86	1.86	2.749(11)	2.739(9)	157	154
O(1W)–H(1WB)...O(1E)	1.81	1.81	2.684(12)	2.671(10)	155	151
O(2W)–H(2WA)...O(1D)	1.86	1.85	2.766(12)	2.765(9)	160	166
O(2W)–H(2WB)...O(5W)	2.07	1.84	2.87(2)	2.77(4)	141	176
O(3W)–H(3WA)...O(1F)	1.82	1.83	2.702(12)	2.714(9)	155	157
O(3W)–H(3WB)...O(1E)#9	1.95	1.90	2.751(12)	2.737(10)	142	147
O(4W)–H(4WA)...O(2A)	2.10	2.00	2.618(13)	2.666(10)	113	127
O(4W)–H(4WB)...O(2C)#8	1.91	1.83	2.750(12)	2.750(9)	147	167
O(1X)–H(1X)...O(2W)#10	2.12	1.98	3.05(4)	2.900(15)	179	167

Symmetry transformations used to generate equivalent atoms: #7 $x+1$, y, z; #8 $x-1$, y, z; #9 $-x+2$, $y-1/2$, $-z+1/2$; #10 $-x+2$, $-y+1$, $-z+1$.

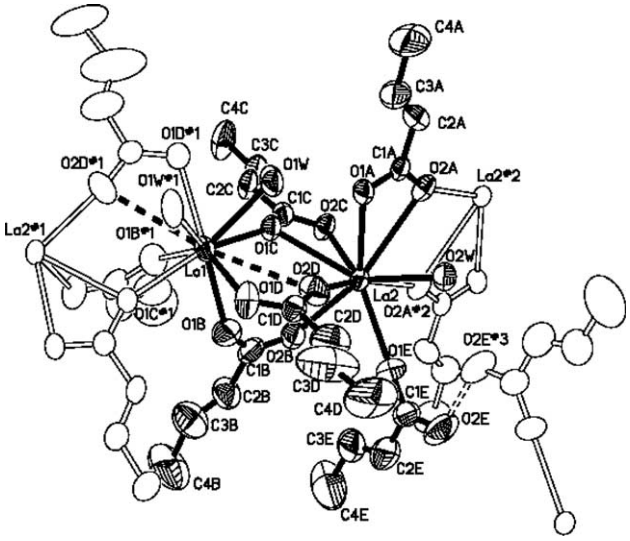

Fig. 1. XP (SHELXL, 1994) diagram of **1**. The asymmetric unit drawn in full thermal ellipsoids at 40% level. As open ellipsoids, the symmetry related atoms showing the way in which the polymer builds up. For symmetry codes, see footnotes in Tables 2 and 3.

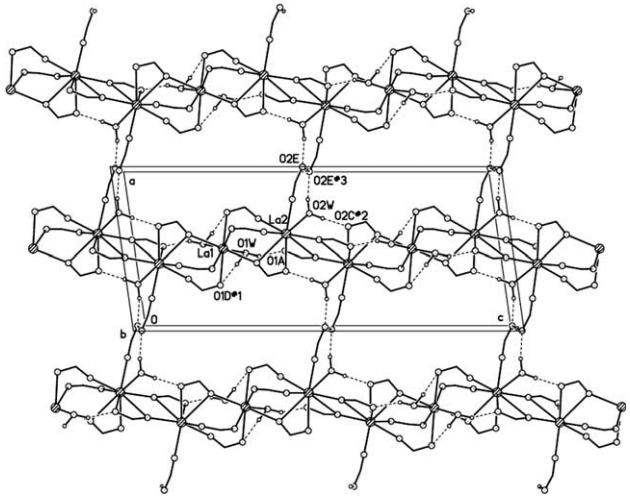

Fig. 2. Packing view of **1** down [0 1 0] showing the H-bonding interactions. For clarity, only the carboxylate groups of the ligands are shown.

protonated in each asymmetric unit, a fact that is clearly incompatible with an ordered structure in it P2/*c*. A detailed look at the packing around O2E shows a short contact O2E...O2E#3 of 2.451(9) Å, which can be attributed to H-bonding interaction between both atoms. Symmetry requirements indicate that the H-atom should lay midway the O2E...O2E#3 distance or offset the center, bonded to one of the oxygen atoms but statistically distributed between both sites. However, since no crystallographic evidence of the presence of the H atom could be obtained, we arbitrarily choose the first option in our calculations.

The structure of compound **2** consists of twisted chains containing two different praseodymium coordination polyhedra evolving along [0 0 1], Fig. 3. Pr1 is 9-coordinated; four bonds are provided by two type d chelating ligands, two from two type b bridging ligands and three aqua molecules. Pr2 is 10-coordinated; eight bonds come from two type c and two type d chelating ligands, and the remaining two from two type d bridging ligands.

A packing view of the structure with chains drawn in projection (coming out of the paper) is shown in Fig. 4. The alkene groups that fill the space between chains are not shown. The H-bonding interactions involving O2W (top, left) are intrachain, while those involving O1W, O3W and the ethanol solvate provide to the link between chains into a 2D structure parallel to [1 0 0], Table 5.

Compounds **3** and **4** are isostructural and crystallize as polymeric chains running along a and therefore only the structure of **3** is shown in Fig. 5. The asymmetric unit consists of two independent Dy metal centers coordinated to six *trans*-2-butenoate anions and four aqua molecules. One hydration water molecule and one *trans*-2-butenoic molecule disordered into a center of symmetry complete both structures. Both cations are 8-coordinate. As in the preceding structure **1**, the long distances shown in broken lines in the figure Ln1...O1C (2.888(10), 2.976(7) Å) and Ln2...O2D (3.154(8), 3.2347(7) Å) are not considered coordination bonds; thus, the Dy–O distances in the DyO_8 cores are slightly

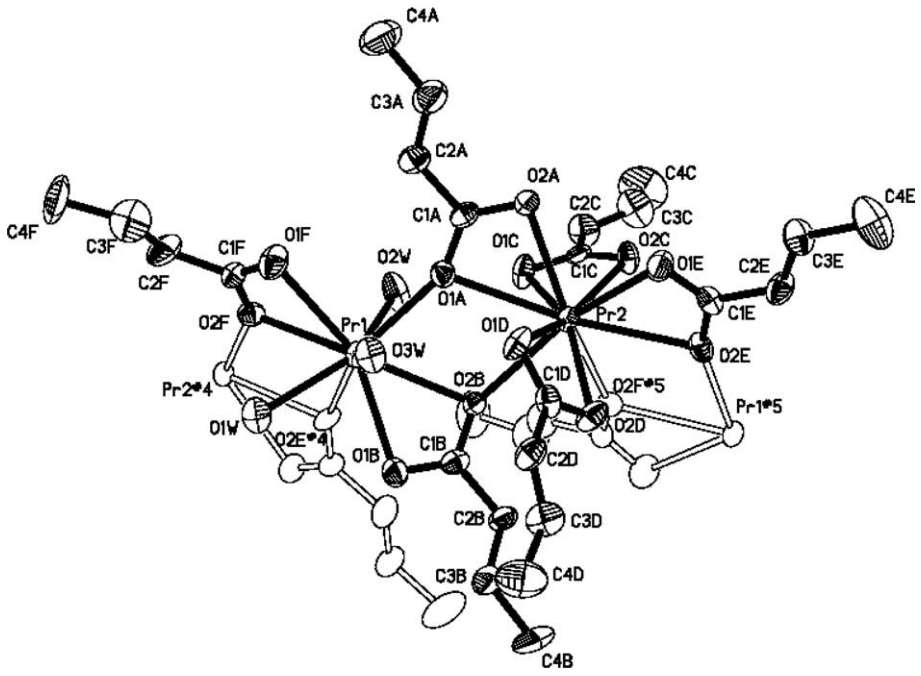

Fig. 3. XP (SHELXL, 1994) diagram of **2**. The asymmetric unit drawn in full thermal ellipsoids at a 40% level. As open ellipsoids, the symmetry related atoms showing the way in which the polymer builds up. For symmetry codes, see footnotes in Tables 4 and 5.

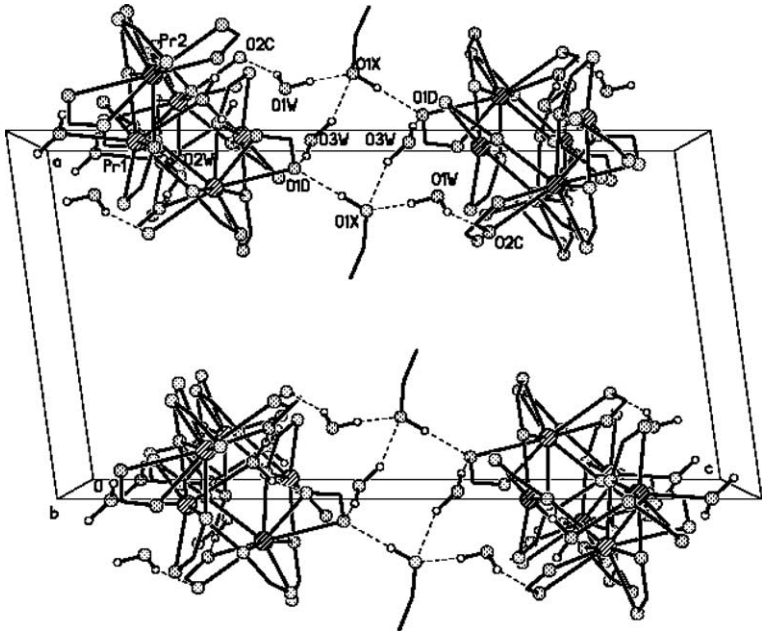

Fig. 4. Packing view of structure **2** down [0 1 0] showing the H-bonding interactions. Alkene groups have been omitted, only the carboxylate groups of the ligands are shown for clarity.

longer than the corresponding Ho–O distances, in accordance with the ''lanthanide contraction'' effect.

Dy1 binds to one type d chelating, two type b and one type d bridging and one type a monodentate ligands plus two aqua molecules, whereas Dy2 binds to one type c chelate, two type b and one type d bridging, a monodentate ligand plus two aqua molecules complete the coordination.

Hydrogen bonding interactions are very important in determining the packing of **3** and **4** in the crystals (Table 7 and Fig. 6). In terms of their effect, they can be classified as ''intra'' or ''inter'' chain bonds. The former

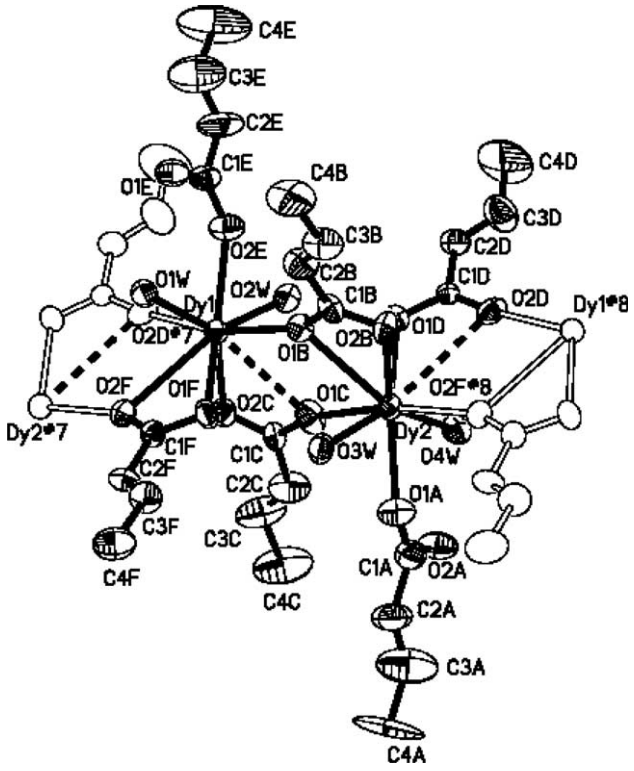

Fig. 5. XP (SHELXL, 1994) diagram of **3**. The asymmetric unit drawn in full thermal ellipsoids at a 40% level. As open ellipsoids, the symmetry related atoms showing the way in which the polymer builds up. The disordered ligand B has been represented by the main fragment. For symmetry codes see footnotes in Tables 6 and 7.

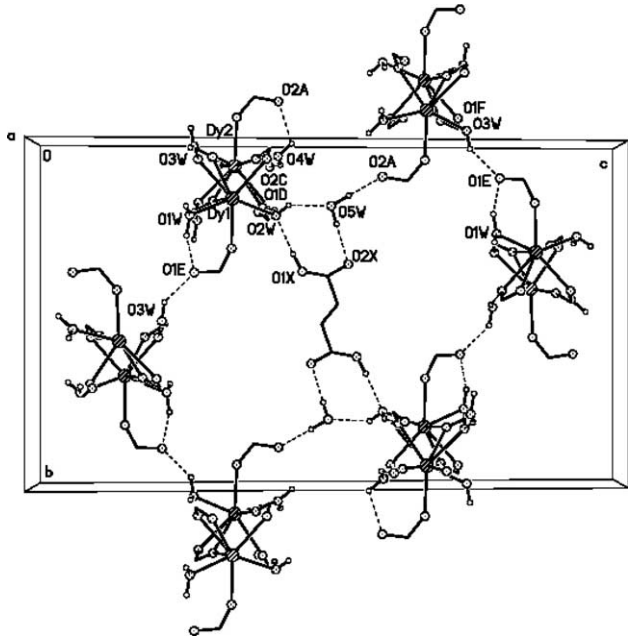

Fig. 6. Packing view of structure **3** down [1 0 0] along the chains direction and showing the H-bonds. Alkene groups have been omitted, only the carboxylate groups of the ligands are shown for clarity.

(those fully involving W1 and W4 and partially W2 and W3, W: water molecule) cooperate in the internal binding of the 1D polymers. The latter, which includes the disordered ligand at the center in Fig. 6, link the chains into a 3D structure.

3.2. Magnetic properties

Fig. 7 shows the thermal variation of the molar magnetic susceptibility χ_M for compound **1**. A temperature independent paramagnetism, of the order of $+260\times10^{-6}$ emu/mol between 100 K and room temperature, is observed after correction of the core electrons contribution (this latter evaluated to -632×10^{-6} emu/mol). A slight increase of χ_M at lower temperature may be due to minute amounts of spurious rare-earth elements present in the starting materials, as it usually occurs in lanthanide-based compounds [20].

Fig. 8 shows the $\chi_M T$ product as a function of temperature, for compound **2**. The room temperature value of $\chi_M T$ is close to 2.5 emu K/mol and decreases continuously by one order of magnitude, as the temperature is lowered. The magnetic moment evaluated from a Curie–Weiss behavior in the temperature range 50–300 K corresponds quite well to the theoretical value expected for a Pr(III) cation (3.43 and 3.58 μ_B, respectively; Table 8). At lower temperature, some deviations to a Curie–Weiss law are expected since praseodymium is a non-Kramers ion with a singlet-type ground state, which is indeed observed below 15 K (inset, Fig. 8).

Fig. 9 shows the temperature dependence of the inverse susceptibility for compounds **3** and **4**. In both cases, the magnetic moments deduced at high temperatures ($T > 20$ and 50 K, for **3** and **4**, respectively) agree perfectly well with the expected values for trivalent rare-earth ions (Table 8). The Weiss parameters (θ values)

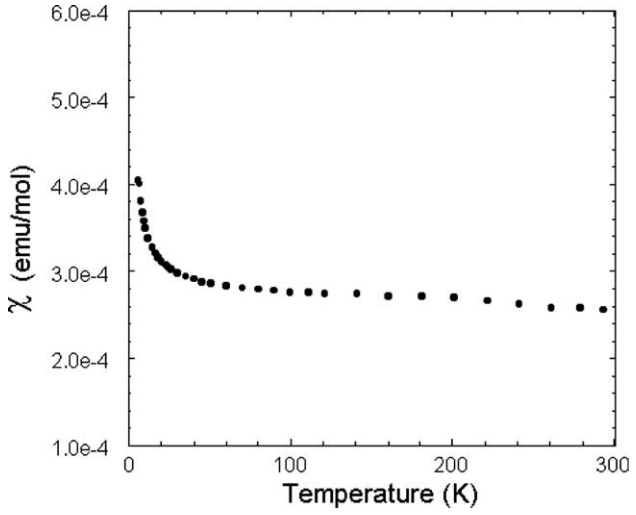

Fig. 7. Molar magnetic susceptibility χ_M of compound **1**, measured under 5 kOe.

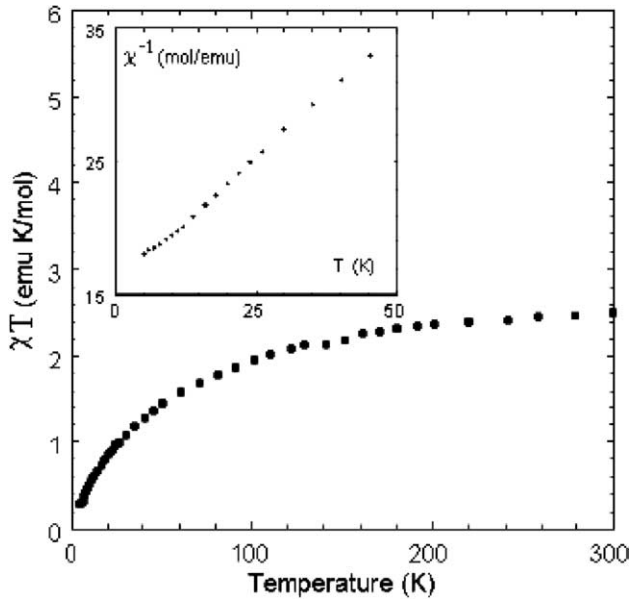

Fig. 8. Temperature dependence of $\chi_M T$ of compound **2**. Inset shows the low temperature region of the inverse susceptibility.

Table 8
Magnetic data for compounds **1**–**4**

Compound		High temperature		Low temperature	
Ln	μ_{theor}	μ_{eff} (μ_B)	θ (K)	μ_{eff} (μ_B)	θ (K)
La	0	$\chi_{(TIP)}$	$\chi_{(300\,K)} = 260 \times 10^{-6}$ (emu/mol)		
Pr	3.58	3.43	−50		
Dy	10.65	10.40	−3	9.26	+0.3
Ho	10.61	10.52	−13	8.4	0

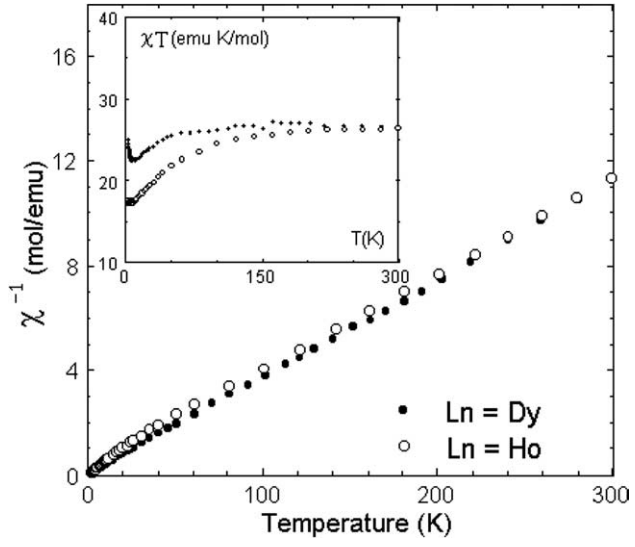

Fig. 9. Inverse magnetic susceptibility of compounds **3** and **4**. Inset shows the temperature dependence of the product $\chi_M T$.

are low (−3 and −13 K, for **3** and **4**, respectively), so the thermal evolution of the product $\chi_M T$ is quite constant at high temperatures. Deviations to the Curie–Weiss behavior occur at low temperatures, yielding reduced values of the effective moment, as tabulated in Table 8. The experimental θ value evaluated in the temperature range 2–10 K is almost zero, within the error bar, although there is a slight tendency to become positive ($\theta \sim +0.3$ K) for the dysprosium-based compound **3**. The decrease of the magnetic moment should be mainly ascribed to crystal field effects, that is, a depopulation of the rare-earth ion Stark components at low temperatures. However, magnetic interactions should not be excluded, since the $\chi_M T$ product of **3** sharply increases below 10 K due to weak ferromagnetic mechanisms, as shown in the inset in Fig. 9. This behavior is also found in the Er-based compound, with a θ value, evaluated at low temperature, of about +1.0 K [21]. Compound **4**, on the other hand, does not show such an increase, staying rather constant in the same temperature range. The difference in behavior regarding these two materials comes from the fact that one (compound **3**) is a Kramers ion with a magnetic doublet as a ground state, while the other (compound **4**) may have a singlet-type fundamental state, due to its non-Kramers nature [22].

4. Conclusions

trans-2-Butenoate is a versatile ligand which coordinates to lanthanides in a variety of ways giving rise to an interesting structural series of binary polymers and oligomers. We report four new compounds of the series based on infinite chains, with the common feature of having two different coordination cores of the metal centers along the chains. Magnetic measurements show that these compounds obey the Curie–Weiss law, with very weak antiferromagnetic interactions in the solids. However, at very low temperatures, range 2–10 K, a slight positive value for θ in **3** suggests that weak ferromagnetic coupling may be operative in the Dy based material.

5. Supplementary material

Crystallographic data (excluding structure factors) have been deposited with the Cambridge Crystallographic Data Centre as supplementary publication Nos. CCDC 249074 **1** (La), CCDC 249075 **2** (Pr), CCDC 249076 **3** (Dy) and CCDC 249077 **4** (Ho). Copies of the data can be obtained free of charge on application to CCDC, 12 Union Road, Cambridge CB2 1EZ, UK (fax: (44) 1223 336-033; e-mail: deposit@ccdc.cam.ac.uk).

Acknowledgments

The authors thank funding by PIP 02568 CONICET, project FONDECIT 102008 and the Spanish Research Council (CSIC) for provision of a free-of-charge license to the CSD system. M.P. is a member of CONICET.

References

[1] T.M. Reineke, M. Eddaoudi, M. O'Keeffe, O.M. Yaghi, Angew. Chem., Int. Ed 38 (1999) 2590.
[2] B.F. Abrahams, B.F. Hoskins, D.M. Michail, R. Robson, Nature 369 (1994) 369, 727.
[3] W. Lin, Z. Wang, L.J. Ma, J. Am. Chem. Soc. 121 (1999) 11249.
[4] O.R. Evans, R. Xiong, G.K. Wong, W. Lin, Angew. Chem., Int. Ed. 38 (1999) 536.
[5] T.M. Reineke, M. Eddaoudi, M. Fehr, D. Kelley, O.M. Yaghi, J. Am. Cem. Soc. 121 (1999) 1651.
[6] L. Ma, O.R. Evans, B.M. Foxman, W. Lin, Inorg. Chem. 38 (1999) 5837.
[7] V. Balzani, N. Sabbatini, F. Scandola, Chem. Rev. 86 (1986) 319.
[8] G.R. Choppin, in: J.-C.G. Bunzli, G.R. Choppin (Eds.), Lanthanide Probes in Life, Chemical and Earth Sciences, Elsevier, Amsterdam, 1989 (Chapter 1).
[9] D. Parker, J.A.G. Williams, J. Chem. Soc., Dalton Trans. (1996) 3613.
[10] C. Benelli, A. Caneschi, D. Gatteschi, L. Pardi, Magnetic Molecular Materials, Kluwer Academic Publishers, 1991, p. 233.
[11] O. Kahn, Molecular Magnetism, VCH, New York, 1993.
[12] B. Barja, P. Aramendia, R. Baggio, M.T. Garland, O. Peña, M. Perec, Inorg. Chim. Acta 355 (2003) 183.
[13] A. Rizzi, R. Baggio, M.T. Garland, O. Peña, M. Perec, Inorg. Chim. Acta 353 (2003) 315.
[14] A.M. Atria, R. Baggio, M.T. Garland, J.C. Muñoz, O. Peña, Inorg. Chim. Acta 357 (2004) 1997.
[15] Bruker. SMART-NT V5.624. Data Collection Software.Siemens Analytical X-ray Instruments Inc., Madison, WI, USA, 2001.
[16] Bruker. SAINT-NT V6.02a. Data Reduction Software. Siemens Analytical X-ray Instruments Inc., Madison, WI, USA, 2000.
[17] G.M. Sheldrick, SHELXS-97 and SHELXL-97. Programs for Structure Resolution and Refinement, University of Göttingen, Germany, 1997.
[18] G.M. Sheldrick, SHELXTL-PC. version 5.0 Siemens Analytical X-ray Instruments, Inc., Madison, WI, USA, 1994.
[19] F.H. Allen, Acta Crystallogr. B58 (2002) 380.
[20] O. Peña, F. Le Berre, J. Padiou, T. Marchand, R. Horyn, A. Wojakowski, J. Solid State Chem. 136 (1998) 160.
[21] Private communication.
[22] A. Herpin, Théorie De Magnetism, Presses Universitaires de France, Paris, 1968.